



HAL
open science

Systematic optical study of high-x In_xGa_{1-x}As/InP structures for infrared photodetector applications

Smiri Badreddine, R.S. Joshya, Demir Ilkay, Saidi Faouzi, Altuntas Ismail, Delphine Lagarde, Cedric Rober, Marie Xavier, Maaref Hassen

► **To cite this version:**

Smiri Badreddine, R.S. Joshya, Demir Ilkay, Saidi Faouzi, Altuntas Ismail, et al.. Systematic optical study of high-x In_xGa_{1-x}As/InP structures for infrared photodetector applications. *Optics and Laser Technology*, 2022, 148, pp.107714. 10.1016/j.optlastec.2021.107714 . hal-03878260

HAL Id: hal-03878260

<https://hal.science/hal-03878260>

Submitted on 8 Jan 2024

HAL is a multi-disciplinary open access archive for the deposit and dissemination of scientific research documents, whether they are published or not. The documents may come from teaching and research institutions in France or abroad, or from public or private research centers.

L'archive ouverte pluridisciplinaire **HAL**, est destinée au dépôt et à la diffusion de documents scientifiques de niveau recherche, publiés ou non, émanant des établissements d'enseignement et de recherche français ou étrangers, des laboratoires publics ou privés.



Distributed under a Creative Commons Attribution - NonCommercial 4.0 International License

Systematic optical study of high-x In_xGa_{1-x}As/InP structures for infrared photodetector applications.

*Smiri Badreddine^{1, 2}, R. S. Joshya¹, Demir Ilkay³, Saidi Faouzi², Altuntas Ismail³
Delphine Lagarde¹, Cedric Rober¹, Marie Xavier¹, Maaref Hassen².*

¹Université de Toulouse, INSA-CNRS-UPS, LPCNO, Toulouse, France

²Université de Monastir, Laboratoire de Micro-Optoélectronique et Nanostructures (LR99ES29), Faculté des Sciences, 5019 Monastir, Tunisia.

³Department of Nanotechnology Engineering and Nanophotonics Research and Application Center, Sivas Cumhuriyet University, 58140 Sivas, Turkey.

Abstract:

Optical and structural properties in high-x In_xGa_{1-x}As ($x > 0.65$) samples with varying indium concentration grown on InP (100) substrate are reported. By increasing the indium fraction, it was found by the high-resolution X-ray diffraction (HR-XRD) study that the dislocation density in the In_xGa_{1-x}As epitaxial layer significantly increased, and the surface quality deteriorated remarkably. Photoreflectance (PR) spectra show the presence of Franz-Keldysh Oscillations (FKOs) features above the In_xGa_{1-x}As energy bandgap. The strain-induced electric field is then estimated directly from the FKOs periods. Temperature-dependent photoluminescence (TDPL) measurements from 10 K to 300 K showed carrier locations (S-shape). This abnormal behavior is due to the dislocation density associated with fluctuations in the indium concentration. A quasi-stationary rate equation model for the temperature-dependent luminescence spectra of the localized state material system is proposed to interpret the band gap emission process quantitatively. Low-temperature (10 K) time-resolved PL measurements show the increase of lifetime with increasing the indium concentration. Yet, the addition of only 1.7% of indium concentration results in a strong enhancement of PL lifetime by ~80%.

All these results reveal a more precise picture of the localization and recombination mechanisms of photogenerated carriers in the InGaAs layer, which could be the crucial factors in controlling the performance of high indium content InGaAs SWIR detector.

Keywords: High-x In_xGa_{1-x}As; dislocation density; S-shaped; FKOs; LSE; localized state; SWIR detector.

Introduction

High- x ($x > 0.53$) $\text{In}_x\text{Ga}_{1-x}\text{As}/\text{InP}$ material systems have achieved great success in optoelectronics and received enormous research interest. One of the most important applications is short-wave (1-3.6 μm) infrared (SWIR) detectors [1] [2], which is required for the various field, such as spectroscopy [3], astronomy [4] and medicine [5]. Yet, in order to extend the response of the detector to longer wavelengths, it is necessary to grow the $\text{In}_x\text{Ga}_{1-x}\text{As}$ alloy with a high In content ($x > 0.53$) [6]. Epitaxial growth requires suitable substrate materials, but lattice mismatch always limits the heteroepitaxy of such materials.

However, the composition of the $\text{In}_x\text{Ga}_{1-x}\text{As}$ layer is very important because it affects the electronic properties of these devices. In order to achieve this goal, the x value in $\text{In}_x\text{Ga}_{1-x}\text{As}$ must be increased to 0.65 to 0.85, which will cause a significant lattice mismatch (+0.55% to +2.2%) between the $\text{In}_x\text{Ga}_{1-x}\text{As}$ layer and the InP substrate [1]. The growth of high- x In is accompanied by the generation of dislocations and other defects caused by lattice mismatch, which will lead to poor surface quality and no uniformity in the alloy composition [7] [8]. For the reasons mentioned above, carriers are captured and redistributed by spatial potential fluctuation and localized energy states, which is referred to as carrier location [9] [10]. Moreover, carrier's localization in semiconductor systems has been extensively studied [11]. Such carrier localization phenomenon usually increases the dark current of the devices [12]. In this framework, Xiaoli et al. [13] have shown that this high dark current is still one of the critical technology issues for the development of extended-wavelength $\text{In}_x\text{Ga}_{1-x}\text{As}/\text{InP}$ ($x > 0.53$) photodetectors (PDs).

The influence of carrier localization is also manifested in the temperature abnormality « S-shape » of the peak PL energy and the form of the low-temperature PL decay curve [14] [15]. In order to fit the curve, several methods have been used, such as double exponential model, triple exponential model, stretched model, etc [16] [17] [18]. Nevertheless, these methods only provide mathematical fitting without detailed physical explanation. Hence, the exact nature of the carrier localization and carrier dynamics are key issues for understanding and improving InGaAs devices. This type of high x $\text{In}_x\text{Ga}_{1-x}\text{As}$ anomalous behavior requires a thorough study to fully explain the physics behind this phenomenon, especially the dark current mechanism. Furthermore, more research is required on both device structure and dark current mechanism of InGaAs photodetectors.

In this letter, we used a luminescence model for localized state ensemble (LSE) developed by Li et al. [17], taking into account generation, thermal activation, and recapturing of excitons by using Pässler model to follow the energy evolution. Moreover, we used the photoreflectance (PR) spectroscopy to obtain important properties of the samples. By analyzing the Franz–Keldysh oscillations, we estimated the built-in electric fields. In addition, time-resolved PL measurements (TRPL) were carried out at 10 K. The investigation of the electronic properties presented in this paper could yield on improvement of the efficiency of the high-x $\text{In}_x\text{Ga}_{1-x}\text{As}/\text{InP}$ structures ($x>0.65$) and make them useful for many types of devices used in optoelectronics and microelectronics.

Experimental details

The three samples, 190 nm-thick $\text{In}_x\text{Ga}_{1-x}\text{As}$ investigated in this paper, were fabricated by Metalorganic Vapor Phase Epitaxy (MOVPE) at 560°C on InP (100) substrate. For the $\text{In}_x\text{Ga}_{1-x}\text{As}$ samples called S1, S2 and S3, it corresponds to $x = 0.650$, $x = 0.661$ and $x = 0.667$ and are described in detail in Ref [7].

The samples were characterized by HR-XRD, PR, PL and TRPL spectroscopy. Then, the samples were characterized by HR-XRD and PL. [The HR-XRD measurements were performed using Rigaku SmartLab diffractometer, equipped with a rotating Cu anode \(wavelength \$K\alpha = 1.54056 \text{ \AA}\$ \) which provides 9 kW X-ray power and four bounced Ge \(220\) monochromator allowing a 2theta precision of \$0.0004^\circ\$.](#) We used a tungsten lamp in PR, and the modulating source an Ar^+ laser (532 nm) chopped at 250 Hz. An InGaAs photodiode detected the PR signal. With PL spectroscopy, we studied the samples between 10 and 300 K while keeping the samples in a closed-cycle helium circulation cryostat. The samples are excited using 514.5 nm line of the continuous-wave Ar^+ laser. The excitation density was fixed at 80 W/cm^2 . The luminescence was dispersed using a JOBIN YVON HRD1 monochromator and detected by a cooled Ge diode detector with a built-in amplifier. The TRPL spectra were measured at a temperature of 8 K using a closed cycle cryostat. In this case, the PL dynamics was excited by a frequency-doubled Ti: Sa laser at $\lambda_{\text{exc}} = 375 \text{ nm}$, the laser-pulse duration was 2 ps pulse-repetition frequency was 4MHz. A super conducting nanowire single photon detector (single quantum) detected the PL signal from the InGaAs samples using a time-correlated single-photon counting system (picotarp from picoquant). The instrument response function is at the order 150 ps. The excitation power is 50 [mW](#), and the laser spot size is about $10 \mu\text{m}^2$).

Results and discussions

1. HR-XRD results

Figure 1 shows the HR-XRD patterns of $\text{In}_x\text{Ga}_{1-x}\text{As}$ epilayer on InP substrate for different indium concentrations. The peaks at 63.5° and 62.2° corresponds to InP and $\text{In}_x\text{Ga}_{1-x}\text{As}$ respectively. Increase of indium content in $\text{In}_x\text{Ga}_{1-x}\text{As}$ epilayer shows a decrease in angle due to the increase of lattice constant [7]. The FWHM of an epilayer examined by HR-XRD is an important parameter to characterize the crystalline quality and dislocation. The values of lattice parameter and dislocation density are calculated and summarized in the Table I. Increase of indium content from $x = 0.650$ to 0.667 shows an increase of the dislocation density from $2.1 \cdot 10^9 \text{ m}^{-2}$ to $3.1 \cdot 10^9 \text{ cm}^{-2}$. However, these values only reflect the average dislocation density of the epilayer. The lattice mismatch has also been determined for different indium content in $\text{In}_x\text{Ga}_{1-x}\text{As}/\text{InP}$. The addition of indium increases the lattice mismatch, but this is significantly less compared to GaAs substrate [19] [20].

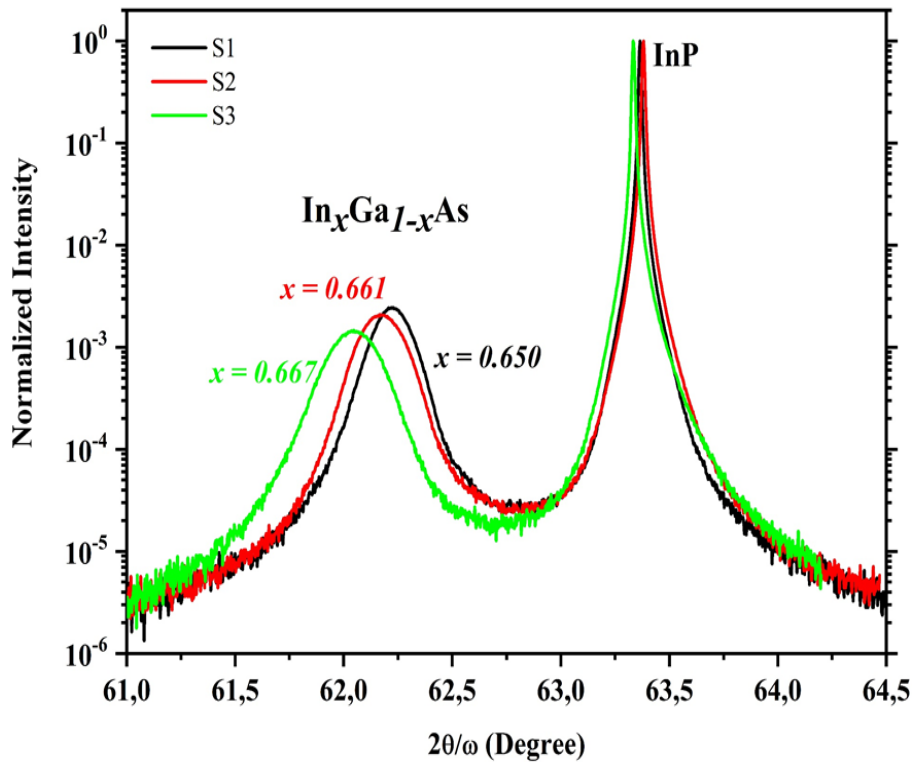


Figure 1: $2\theta/\omega$ HR-XRD spectra of the $\text{In}_x\text{Ga}_{1-x}\text{As}$ layers having different In alloys grown on InP by MOVPE [7].

Samples	Indium ($x =$)	Lattice parameter (\AA)	Dislocation density (10^9cm^{-2}) [7]	Lattice mis- match (%)
S1	0.650	5.9545	2.1	1.44
S2	0.661	5.9592	2.6	1.54
S3	0.667	5.9618	3.1	1.58

Table I: $\text{In}_x\text{Ga}_{1-x}\text{As}$ samples characteristics and calculated parameters using HR-XRD.

2. Photoreflectance results

The photoreflectance technique (PR) is an important and useful tool to investigate and qualify the interband transitions and electric field distributions in semiconductor and multilayer structures because of its derivatives-like nature and sharp spectral features. The main advantage of PR is its high sensitivity, even at room temperature. However, the existence of overlapping spectral characteristics of different regions of multilayer structures can complicate PR analysis.

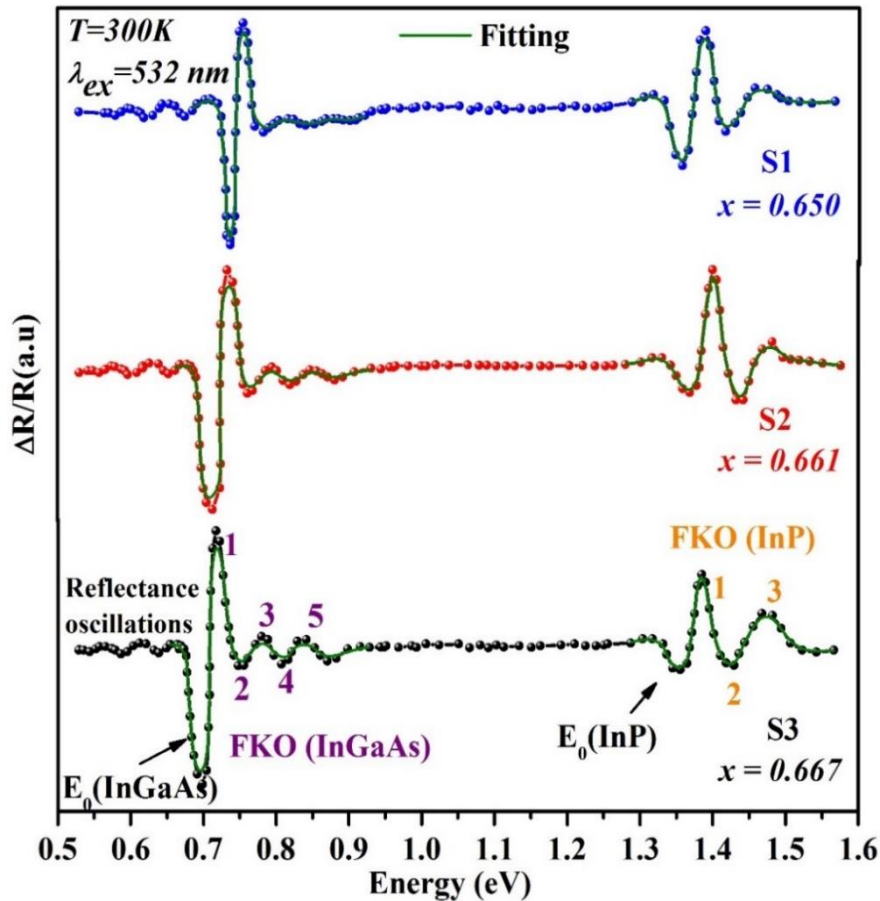


Figure 2: Room temperature PR spectra (dots) obtained from samples S1, S2 and S3 at different indium concentration and fits (green lines) performed using Eq. ~1.

Figure 2 shows the PR spectra of the three high-x In_xGa_{1-x}As samples at room temperature. PR is a differential form of reflectance; therefore, its sensitivity is very high, as shown in figure 2. In this case, transitions originating from the InP substrate and InGaAs layer are visible [21] [22]. In addition, the PR spectra reveal many oscillations above the high-x In_xGa_{1-x}As layer and InP substrate for the three samples [23] [24]. These oscillations are related to the Franz-Keldysh oscillations (FKO), resulting from an electric field present in the different samples. FKO has a regular periodicity and presents only the energies above the critical point [25]. There appear to be two sets of FKOs, one related to the InP gamma-point of 1.39 (± 0.02) eV and the other linked with the InGaAs bandgap. Note that the shape and position of the PR spectrum in all samples are not identical. The shift in the extrema of the FKOs is observed. This is due to the variation of lattice mismatch between the InGaAs layer and the InP substrate, increasing the indium content in In_xGa_{1-x}As. The FKOs have been frequently used to define the built-in electric field inside the semiconductor device. In this article, we will only be interested in this FKO related to the InGaAs layer.

Now, to estimate the value of electric fields in the high-x In_xGa_{1-x}As layer, the FKO period is analyzed using an asymptotic expression for the PR line shape given by Aspnes and Studna [26]. In the region 0.7-0.9 eV, the oscillatory ΔR/R signal can be described by:

$$\frac{\Delta R}{R} = \frac{1}{E^2(E-E_0)} \exp \left[-2(E-E_0)^{\frac{1}{2}} \frac{\Gamma}{(\hbar\Omega)^{\frac{3}{2}}} \right] \cos \left[\frac{4}{3} \left(\frac{E-E_0}{\hbar\Omega} \right)^{\frac{3}{2}} + \phi \right] \quad (1)$$

where Γ is the broadening parameter, φ is an arbitrary phase factor and ħΩ is the electro-optic energy expressed as follows:

$$\hbar\Omega = \left(\frac{q^2 \hbar^2 \text{Fint}^2}{8\mu} \right)^{1/3} \quad (2)$$

Note that q is the electron charge, μ is the reduced inter-band effective mass in the electric field direction and Fint is the internal electric field.

In order to extract PR parameters (Fint, ħΩ, etc.), the energy of FKO extrema (E_n) is given by [27]:

$$E_n = (\hbar\Omega)H_n + E_0 \quad (3)$$

and

$$H_n = \left[\left(\frac{3\pi}{2} \right) (n - 1/2) \right]^{2/3} \quad (4)$$

Thus, by plotting E_n as a function of H_n (see figure 3), from linear fitting, we can determine $\hbar\Omega$ and E_0 from the slope and the intersection with the ordinate at the origin, respectively. Recalling equation 2, F_{int} can be extracted by:

$$F_{\text{int}} = \sqrt{\frac{2\mu(\hbar\Omega)^2}{q^2\hbar^2}} \quad (5)$$

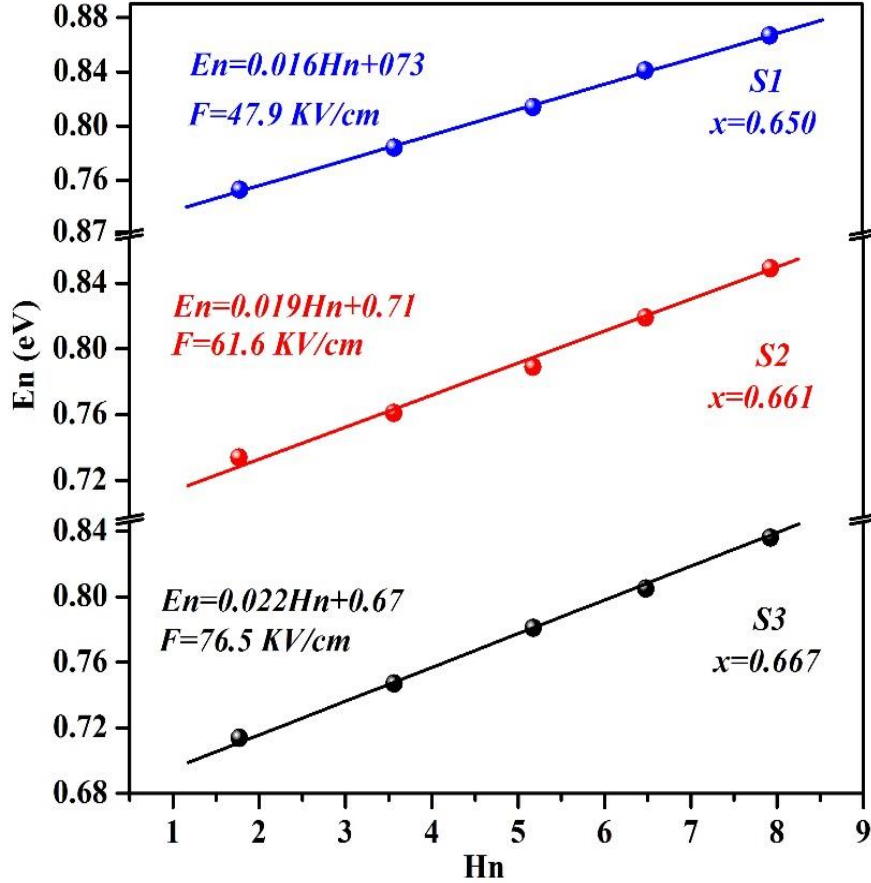


Figure 3: Plot of the energy extremes E_n vs. index number H_n for each sample. The straight lines are fittings to the FKO model using eq.3. The lines slope and ordinates to origin relate to the electric field strength F_{int} and the InGaAs bandgap energy E_0 .

A summary of the experimental results is shown in table II. The obtained values of E_0 are 0.73, 0.71 and 0.67 eV for sample S1, S2 and S3, respectively. InGaAs band gap value is close to that obtained by HR_XRD measurements. To evaluate Γ for the InGaAs transitions, experimental linewidths are least-squares fits equation 1 as shown in figure 2. It is interesting to note that the values Γ increase with increasing indium concentration in $\text{In}_x\text{Ga}_{1-x}\text{As}$. However, we can see significant differences in the internal electric field strength in the samples. It is important to note that sample S3 with the highest residual strain presents the highest internal electric field of 76.5 kV/m. According to D. Yan et al. [28], the value of the internal electric field in the ternary alloy semiconductor ($\text{In}_{0.53}\text{Ga}_{0.47}\text{As}$), lattice-matched to InP substrate is

30 kV/cm. Yet, for the sample S1, S2 and S3, the residual strain in epitaxial layers increases with the increase of indium concentration. As all the structures examined in this paper have the same geometric structure, we believe that the significant difference in the electric fields is due to different amounts of dislocation density. A high concentration of dislocation density will reduce the quality of the structure, form electron dispersion centers, and generate a strong built-in electric field in the sample.

Sample	x_{In}	E_0 (eV)	Γ (meV)	$\hbar\Omega$ (meV)	F_{int} (kV/cm)	
					Exp	Ref.
S1	0.650	0.73 ± 0.02	3.2 ± 0.1	16 ± 1	47.9 ± 0.2	$F=155 \pm 5$ ($x_{\text{In}}=0.15$) [29]
S2	0.661	0.71 ± 0.02	4.9 ± 0.1	19 ± 1	61.6 ± 0.2	$F=30 \pm 2$ ($x_{\text{In}}=0.53$) [28]
S3	0.667	0.67 ± 0.02	5.1 ± 0.1	22 ± 1	76.5 ± 0.2	$F= 50$ ($x_{\text{In}}=0.65$) [30]

Table II: Summary of PR results for $\text{In}_x\text{Ga}_{1-x}\text{As}$ layers. Bandgap energy E_0 , broadening Γ , internal electric field F_{int} , and electro-optical energy $\hbar\Omega$. Some value from the literature are added.

3. Photoluminescence results:

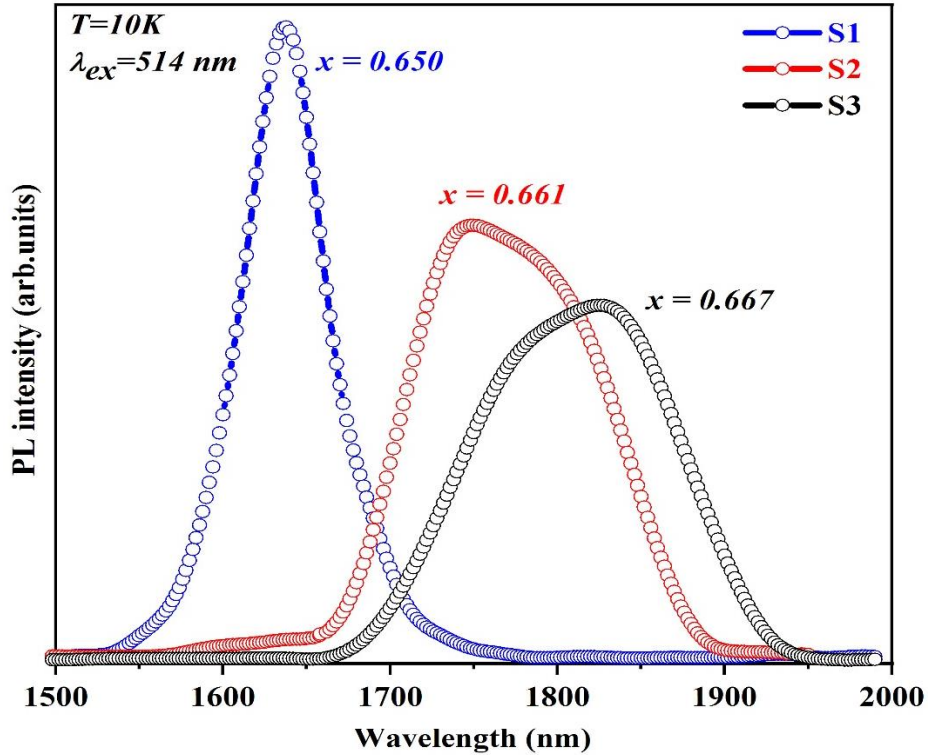


Figure 4: Comparison of the PL spectra of the three InGaAs samples with different In concentrations at 10K.

Figure 4 compares the PL spectra of the $\text{In}_x\text{Ga}_{1-x}\text{As}$ epilayer with various indium concentrations ($x = 0.650, 0.661, 0.667$) at 10 K under the same excitation power density of 80 W/cm^2 of 514 nm. As indium concentration increases to a small amount of 1.7%, the PL peak shows a large red-shift of about 170 nm, which is most suitable for short-wave infrared applications. The FWHM of the PL emission increases significantly with increasing indium concentration in $\text{In}_x\text{Ga}_{1-x}\text{As}$: incorporating high indium in $\text{In}_x\text{Ga}_{1-x}\text{As}$ induces the structural in-homogeneities that cause localized potential fluctuations in its band structure [31] [32]. Also, as shown in figure 5, the PL peak energy as a function of lattice temperature shows a “S-shape” (red/blue/red-shift) behavior which is the footprint of the presence of localized carriers [7]. The S-shape behavior becomes more pronounced at high indium concentration. The phenomenon of the S-shape behavior at low temperature can be explained as follows : at cryogenic 10 K (*party I in figure 6*), the excitons are strongly located in levels whose energy distribution extends within the band gap of the material. As lattice temperature to $\sim 60 \text{ K}$, excitons thermalize and relax to the local minima (alloy disorder) so that the PL peak energy decreases and we observed the first red shift. With further increase of temperature from 60 K to 100 K (*party II in figure 6*), the localized carriers gain enough thermal energy to be transferred to higher energy levels in the band-tails until they reaches maximum of band continuum, thus leading to blue-shift of the PL peak energy. Finally, when the lattice temperature increased above 100K (*party III in figure 6*), the carriers are thermally activated and prevented from localization (free carrier recombination). A schematic diagram is shown in figure 6. The classic models such as Varshni [16], Vina [17], and Pässler [18] explain well the behavior at high temperature but unable to reproduce it at low temperature. The localized effects at low temperature can be explained using the Localized State Exciton Model or modified Pässler model with the impact of thermal redistribution of localized carriers [33] [34] [35]:

$$E(T) = E(0) - \frac{\alpha\theta}{2} \left[\sqrt{1 + \left(\frac{2T}{\theta}\right)^2} - 1 \right] - x(T) \cdot K_B \cdot T \quad (6)$$

The second term describes the shrinking of band according to the classic Pässler equation with α and Θ are Varshni parameter and the Debye temperature, respectively. The dimensionless coefficient $x(T)$ can be obtained by numerically solving the equation [36]:

$$x e^x = \left[1 + \left(\frac{\sigma}{K_B \cdot T} \right)^2 - x \right] \left(\frac{\tau_r}{\tau_{nr}} \right) e^{\frac{E_0 - E_a}{K_B \cdot T}} \quad (7)$$

where σ is the broadening parameter for the distribution of the localized states at central energy E_0 . τ_r , τ_{nr} , E_a and K_B are the radiative lifetime, non-radiative lifetime, activation energy, and

the Boltzmann constant. At high temperature, the solution of equation 7 can be approximated to be:

$$x \left(\frac{\sigma}{k_B T} \right)^2 \quad (8)$$

Equation 6 can be rewritten as [10]:

$$E(T) = E(0) - \frac{\alpha\theta}{2} \left[\sqrt{1 + \left(\frac{2T}{\theta} \right)^2} - 1 \right] - \frac{\sigma^2}{k_B T} \quad (9)$$

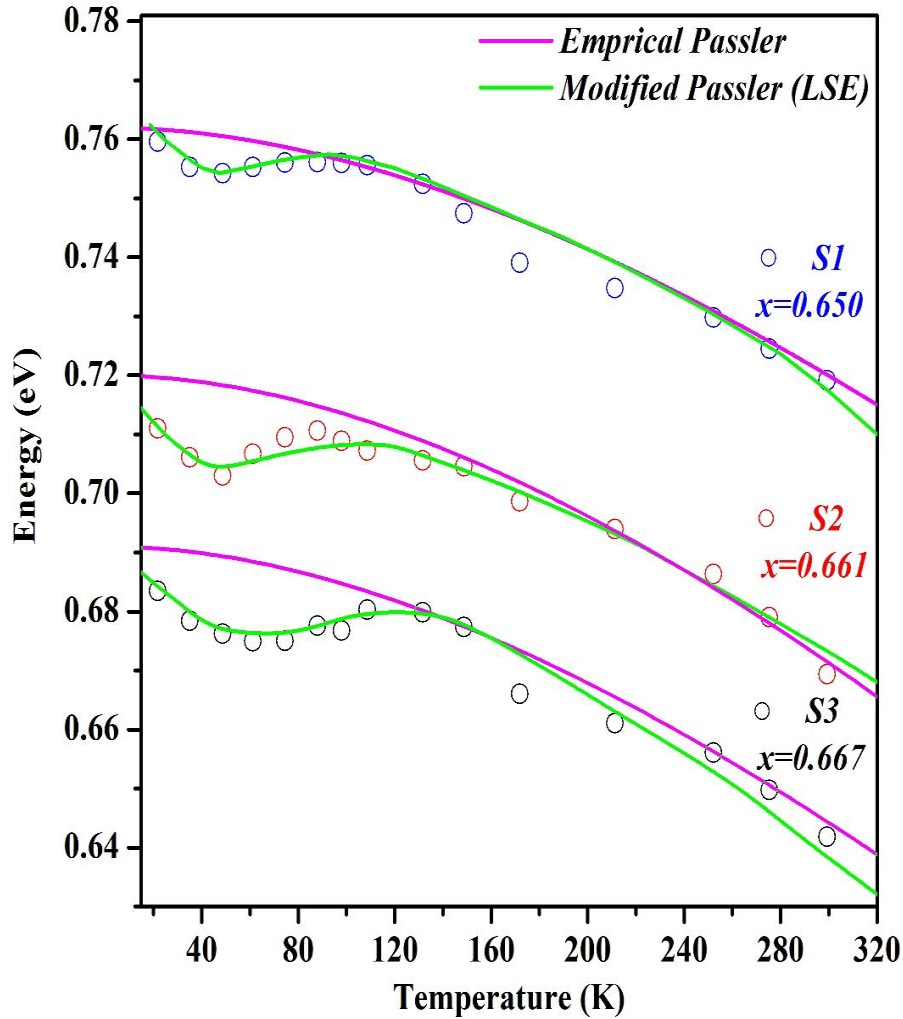


Figure 5: The PL peak energy of $\text{In}_x\text{Ga}_{1-x}\text{As}$ epilayer as a function of lattice temperature. green and red solid lines describes the classical and modified Pässler model fit to the experimental data respectively. The parameters yielding to the best fit are tabulated in Table III.

Figure 5 shows compares the experimental data with the classical and modified Pässler Model. The modified Pässler model gives a good agreement with experimental data. The fitting parameters are summarized in table III.

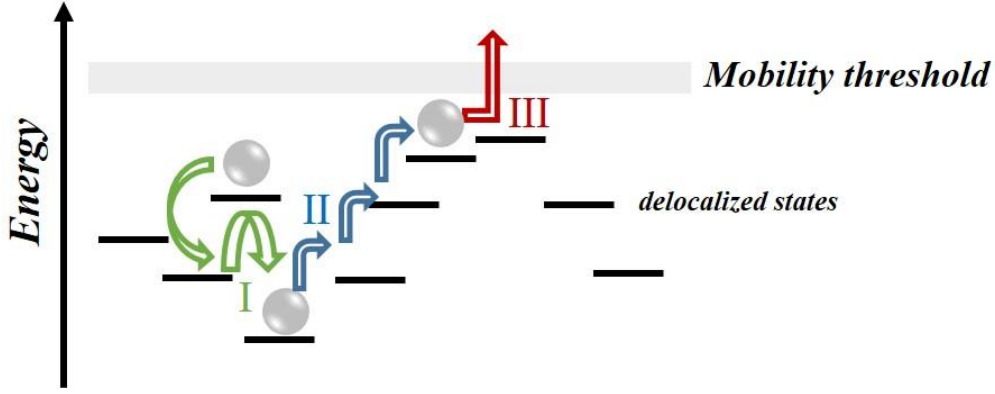


Figure. 6: Schematic diagram for describing the hopping of carriers in localized levels. Dotted lines I, II and III indicate the transition process of carriers between different localization states with increasing temperatures.

Samples	x_{In}	E_0 (meV)	$E_a - E_0$ (meV)	σ (meV)	τ_r / τ_{tr}	α (eV/k)	T (k)
S1	0.650	0.76	16.70	4.8	2000	2.70	200
S2	0.661	0.71	24.26	11.0	1500	2.73	185
S3	0.667	0.68	29.30	16.5	535	2.60	243

Table III: The best-fit parameters of the experimental data of $In_xGa_{1-x}As$ for different In content, obtained by the modified Pässler model.

Using the LSE model, the temperature dependence of the position of the PL peaks of the three S-shaped structures can be well reconstructed, as shown in figure 5. From the calculation, we obtained the same E_0 value as obtained by PR results. However, $\Delta E = E_a - E_0$ is a necessary parameter to understand the abnormal temperature dependence of temperature better. From a physical point of view, there are two situations. ΔE can be positive (+) or negative (-), but ΔE is usually positive. In our case, it is positive and it increases by increasing the indium concentration. For samples S3, S2, and S1, the values are 16.5 meV, 11.0 meV, and 4.8 meV, respectively, that is, E_a is located above E_0 . In this case, the localized carriers are thermally activated to a higher energy state. This is why the S-shape is more evident in the S3 sample. This explains the larger occupied localized states and the proximity of empty states located at 10 K. In fact, the excitons gain enough thermal energy to overcome the small barrier and excite to a higher localized state above E_a with larger potential. The depth of potential fluctuation assigned by σ is the result of fluctuations in the indium composition and the presence of the electric field in our structures [32]. The potential depth is found to be 10.5; 15.0 and 16.8 meV. It is larger with increasing concentration indium and electric-field. As a

result, we can see that the increase of potential depth increases the dark current of the devices, which could be the crucial factor in controlling the performance of high indium content $\text{In}_x\text{Ga}_{1-x}\text{As}$ SWIR detector [37].

4. TRPL results

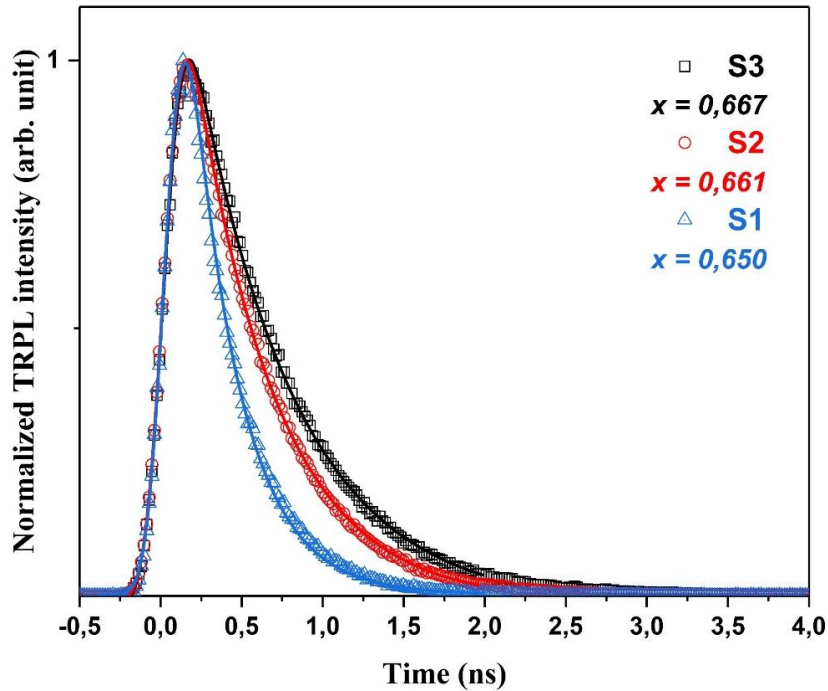


Figure 7: Normalized TRPL decay curves for $\text{In}_x\text{Ga}_{1-x}\text{As}/\text{InP}$ samples for $x=0.65$ to 0.667 at 10K with excitation power $50 \mu\text{W}$. A single exponential decay (solid line) fitted with experimental data (symbols).

Time-resolved photoluminescence measurement was carried out to understand the influence of indium concentration on the carrier dynamics in the high- x $\text{In}_x\text{Ga}_{1-x}\text{As}$ layers. The PL lifetime profile of $\text{In}_x\text{Ga}_{1-x}\text{As}$ at 10K for different indium concentrations are shown in figure 7. To obtain the PL lifetime, we fitted with a single-exponential decay, $I(t) = I_0 * \exp(-\frac{t}{\tau})$ [38] where I_0 and τ are amplitude and decay time-constant, respectively. The lifetime is determined to be 0.33 ns , 0.49 ns , and 0.59 ns for the sample S1, S2, and S3, respectively [39]. Surprisingly, the low PL lifetime of 0.33 ns is obtained in sample S1, which has the best crystalline quality compared to the others. The addition of only 1.7% of indium concentration results in a strong enhancement of PL lifetime by $\sim 80\%$. Regarding this increase of lifetime with increasing the indium concentration, two factors should be considered: the localization of excitons and the local electric field. It is well known that the localization of excitons yields an increase in the radiation lifetime [40]. This could explain that the decay time in sample S3 is longer than the one in sample S1 as the excitons could be strongly localized. The larger

electric-field in the high-In structures could also lead to a spatial separation of electrons and holes, yielding an increase in recombination time [41].

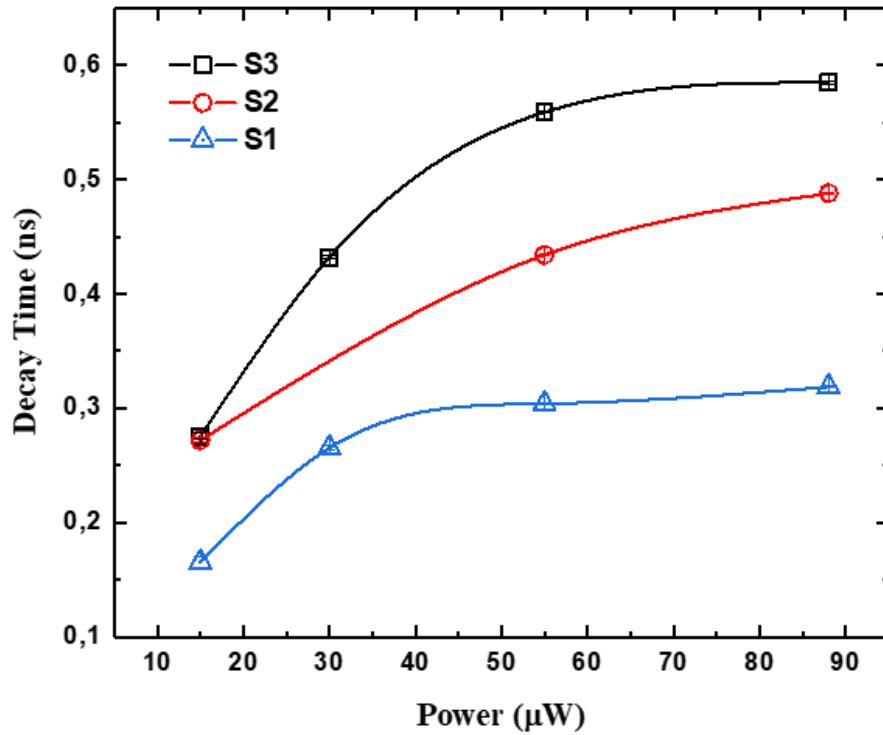


Figure. 8: PL lifetime as a function of excitation power (μW) of the $\text{In}_x\text{Ga}_{1-x}\text{As}/\text{InP}$ samples for $x=0.65$ to 0.667 at 10K

Figure 8 shows the measured PL lifetime τ_{InGaAs} vs. the pump power for an excitation wavelength of 375 nm . The PL lifetime of the $\text{In}_x\text{Ga}_{1-x}\text{As}$ first increases and then saturates for pump powers beyond $60\ \mu\text{W}$. This could be due to the filling and saturation of localized states. Then, at high density of carriers, the free excitons could be more sensitive to the local electric field, yielding an increase of the recombination time. This hypothesis should be confirmed by further investigations [42].

Conclusion

We have studied high- x $\text{In}_x\text{Ga}_{1-x}\text{As}$ layers on InP substrates by HR-XRD, PL, PR and TRPL with varying indium concentration. PR measurement revealed oscillations above the InGaAs layer, which are related to the Franz-Keldysh oscillations (FKO). From an analysis of the FKO, we have estimated that the electric field increases with indium concentration. The temperature-dependent PL measurement demonstrates the critical role played by carrier localization. The S-shape behavior is the result of a competitive process between localized and non-localized carriers. For increasing indium concentration in InGaAs , the density of

localization increases. Luminescence measurements have been successfully modeled and interpreted using the developed LSE model. These theoretical studies have quantitatively explained the temperature-dependent spectra observed. LT-TRPL measurements showed longer decay times in the high-x samples, which is likely due to increased localization and electric field effects.

Our works shows that the high defect densities leads the carrier's localization, thereby increasing the dark current of the device. In addition, it's imparts a deep level understanding of the behavior of carriers and optoelectronic parameters in high-x $\text{In}_x\text{Ga}_{1-x}\text{As}$ structures. In the next work, we will study the compensation of the strain layer by adding the buffer layer in our high-x $\text{In}_x\text{Ga}_{1-x}\text{As}$ structures for minimizing the dislocation density and the residual strain (ϵ) in the $\text{In}_x\text{Ga}_{1-x}\text{As}$ epitaxial layer.

Acknowledgments

This work was supported by the University of Monastir, Laboratory of Micro-Optoelectronics and Nanostructures (LMON), Faculté des Sciences, 5019, Monastir, Tunisia and by the University of Toulouse, INSA-CNRS-UPS, LPCNO, Toulouse, France.

References

- [1] P. Jurczak, K. A. Sablon, M. Gutiérrez, H. Liu, et J. Wu, « 2.5- μm InGaAs photodiodes grown on GaAs substrates by interfacial misfit array technique », *Infrared Phys. Technol.*, vol. 81, p. 320-324, mars 2017, doi: 10.1016/j.infrared.2017.02.001.
- [2] J. Zhang, M. A. Itzler, H. Zbinden, et J.-W. Pan, « Advances in InGaAs/InP single-photon detector systems for quantum communication », *Light Sci. Appl.*, vol. 4, n° 5, Art. n° 5, mai 2015, doi: 10.1038/lsa.2015.59.
- [3] I. Demir, I. Altuntas, B. Bulut, M. Ezzedini, Y. Ergun, et S. Elagoz, « Comprehensive growth and characterization study on highly n-doped InGaAs as a contact layer for quantum cascade laser applications », *Semicond. Sci. Technol.*, vol. 33, n° 5, p. 055005, avr. 2018, doi: 10.1088/1361-6641/aab9d3.
- [4] C. L. Tan et H. Mohseni, « Emerging technologies for high performance infrared detectors », *Nanophotonics*, vol. 7, n° 1, p. 169-197, janv. 2018, doi: 10.1515/nanoph-2017-0061.
- [5] X. Ji *et al.*, « Deep-level traps induced dark currents in extended wavelength $\text{In}_x\text{Ga}_{1-x}\text{As/InP}$ photodetector », *J. Appl. Phys.*, vol. 114, n° 22, p. 224502, déc. 2013, doi: 10.1063/1.4838041.
- [6] L. Zhao, Z. Guo, M. Zhang, S. Yang, et L. Zhao, « Surface-interface analysis of $\text{In}_x\text{Ga}_{1-x}\text{As/InP}$ heterostructure in positive and negative mismatch system », *Surf. Interface Anal.*, vol. 51, n° 5, p. 498-505, mai 2019, doi: 10.1002/sia.6609.
- [7] B. Smiri *et al.*, « Optical and structural properties of In-rich $\text{In}_x\text{Ga}_{1-x}\text{As}$ epitaxial layers on (1 0 0) InP for SWIR detectors », *Mater. Sci. Eng. B*, vol. 262, p. 114769, déc. 2020, doi: 10.1016/j.mseb.2020.114769.
- [8] T. Asar, S. Özçelik, et E. Özbay, « Structural and electrical characterizations of $\text{In}_x\text{Ga}_{1-x}\text{As/InP}$ structures for infrared photodetector applications », *J. Appl. Phys.*, vol. 115, n° 10, p. 104502, mars 2014, doi: 10.1063/1.4868056.
- [9] J. A. del Alamo, « Nanometre-scale electronics with III-V compound semiconductors », *Nature*, vol. 479, n° 7373, p. 317-323, nov. 2011, doi: 10.1038/nature10677.
- [10] B. Smiri, T. Hidouri, F. Saidi, et H. Maaref, « Carriers' localization and thermal redistribution in InAlAs/InP grown by MOCVD on (311)A- and (311)B-InP substrates », *Appl. Phys. A*, vol. 125, n° 2, p. 134, févr. 2019, doi: 10.1007/s00339-019-2444-9.
- [11] Wei *et al.* « Carrier Localization Effects in InGaN/GaN Multiple-Quantum-Wells LED Nanowires: Luminescence Quantum Efficiency Improvement and “Negative” Thermal Activation Energy », *Scientific Reports*, vol. 6, no 34545, p. 1087, sep. 2016, doi: 10.1038/srep34545
- [12] B. Du *et al.*, « Improved performance of high indium InGaAs photodetectors with InAlAs barrier », *Jpn. J. Appl. Phys.*, vol. 57, n° 6, p. 060302, juin 2018, doi: 10.7567/JJAP.57.060302.

- [13] L. Zhao, Z. Guo, M. Zhang, S. Yang, et L. Zhao, « Surface-interface analysis of $\text{In}_x\text{Ga}_{1-x}\text{As}/\text{InP}$ heterostructure in positive and negative mismatch system », *Surf. Interface Anal.*, vol. 51, n° 5, p. 498-505, mai 2019, doi: 10.1002/sia.6609.
- [14] B. Smiri, I. Fraj, F. Saidi, R. Mghaieth, et H. Maaref, « Effect of piezoelectric field on type II transition in InAlAs/InP (311) alloys with different substrate polarity », *J. Alloys Compd.*, vol. 736, p. 29-34, mars 2018, doi: 10.1016/j.jallcom.2017.11.121.
- [15] B. Smiri, F. Saidi, A. Mlayah, et H. Maaref, « Power- and temperature-dependent photoluminescence investigation of carrier localization at inverted interface transitions in InAlAs/InP structures », *Jpn. J. Appl. Phys.*, vol. 59, n° 2, p. 022001, janv. 2020, doi: 10.7567/1347-4065/ab65a6.
- [16] Y. P. Varshni, « Temperature dependence of the energy gap in semiconductors », *Physica*, vol. 34, n° 1, p. 149-154, janv. 1967, doi: 10.1016/0031-8914(67)90062-6.
- [17] L. Viña, S. Logothetidis, et M. Cardona, « Temperature dependence of the dielectric function of germanium », *Phys. Rev. B*, vol. 30, n° 4, p. 1979-1991, août 1984, doi: 10.1103/PhysRevB.30.1979.
- [18] R. Pässler, « Basic Model Relations for Temperature Dependencies of Fundamental Energy Gaps in Semiconductors », *Phys. Status Solidi B*, vol. 200, n° 1, p. 155-172, 1997, doi: [https://doi.org/10.1002/1521-3951\(199703\)200:1<155::AID-PSSB155>3.0.CO;2-3](https://doi.org/10.1002/1521-3951(199703)200:1<155::AID-PSSB155>3.0.CO;2-3).
- [19] R. Deki, T. Sasaki, et M. Takahasi, « Strain relaxation and compositional separation during growth of $\text{InGaAs}/\text{GaAs}(001)$ », *J. Cryst. Growth*, vol. 468, p. 241-244, juin 2017, doi: 10.1016/j.jcrysgro.2017.01.028.
- [20] G. P. Dimitrakopoulos *et al.*, « Misfit dislocation reduction in InGaAs epilayers grown on porous GaAs substrates », *Appl. Surf. Sci.*, vol. 306, p. 89-93, juill. 2014, doi: 10.1016/j.apsusc.2014.02.117.
- [21] J. P. Estrera, W. M. Duncan, Y. C. Kao, H. Y. Liu, P. D. Stevens, et E. A. Beam III, « Systematic optical study of $\text{In}_x\text{Ga}_{1-x}\text{As}$ on InP using photoluminescence, photorefectance, and micro-Raman spectroscopy », Somerset, NJ, juill. 1992, p. 120, doi: 10.1117/12.60447.
- [22] C.-C. Chang, M.-S. Hsu, Y. Ouyang, et Y.-C. Wang, « Optical properties of the modulation doped $\text{InGaAs}/\text{InAlAs}$ quantum well », in *Photonic Fiber and Crystal Devices: Advances in Materials and Innovations in Device Applications III*, août 2009, vol. 7420, p. 74200S, doi: 10.1117/12.825660.
- [23] R. Nedzinskas *et al.*, « Polarized photorefectance and photoluminescence spectroscopy of $\text{InGaAs}/\text{GaAs}$ quantum rods grown with As_2 and As_4 sources », *Nanoscale Res. Lett.*, vol. 7, n° 1, p. 609, nov. 2012, doi: 10.1186/1556-276X-7-609.
- [24] N. Tounsi, M. M. Habchi, Z. Chine, A. Rebey, et B. El Jani, « Optical properties study of $\text{In}_{0.08}\text{Ga}_{0.92}\text{As}/\text{GaAs}$ using spectral reflectance, photorefectance and near-infrared Photoluminescence », *Superlattices Microstruct.*, vol. 59, p. 133-143, juill. 2013, doi: 10.1016/j.spmi.2013.04.009.

- [25] X. Chen, K. Wang, et M. C. Beard, « Ultrafast probes at the interfaces of solar energy conversion materials », *Phys. Chem. Chem. Phys.*, vol. 21, n° 30, p. 16399-16407, juill. 2019, doi: 10.1039/C9CP02768H.
- [26] D. E. Aspnes et A. A. Studna, « Schottky-Barrier Electroreflectance: Application to GaAs », *Phys. Rev. B*, vol. 7, n° 10, p. 4605-4625, mai 1973, doi: 10.1103/PhysRevB.7.4605.
- [27] B. Smiri, I. Fraj, M. Bouzidi, F. Saidi, A. Rebey, et H. Maaref, « Effect of V/III ratio on the optical properties of (3 1 1)A and (3 1 1) B oriented InAlAs/InP heterostructures », *Results Phys.*, vol. 12, p. 2175-2182, mars 2019, doi: 10.1016/j.rinp.2019.02.035.
- [28] D. Yan *et al.*, « Photorefectance characterization of an InP/InGaAs heterojunction bipolar transistor structure », *Appl. Phys. Lett.*, vol. 61, n° 17, p. 2066-2068, oct. 1992, doi: 10.1063/1.108308.
- [29] C.-H. Ho, K.-W. Huang, Y.-S. Lin, et D.-Y. Lin, « Practical photoluminescence and photorefectance spectroscopic system for optical characterization of semiconductor devices », *Opt. Express*, vol. 13, n° 11, p. 3951-3960, mai 2005, doi: 10.1364/OPEX.13.003951.
- [30] W. Zhou *et al.*, « Photorefectance Characterization of the Semi-Insulating InP Substrate Interface with InGaAs and InAlAs Epilayers », *MRS Proc.*, vol. 281, janv. 2011, doi: 10.1557/PROC-281-121.
- [31] B. Tongbram, S. Sengupta, et S. Chakrabarti, « Impact of an $\text{In}_x\text{Ga}_{1-x}\text{As}$ Capping Layer in Impeding Indium Desorption from Vertically Coupled InAs/GaAs Quantum Dot Interfaces », *ACS Appl. Nano Mater.*, vol. 1, n° 8, p. 4317-4331, août 2018, doi: 10.1021/acsanm.8b01170.
- [32] I. Fraj, T. Hidouri, F. Saidi, et H. Maaref, « Carrier localization in $\text{In}_{0.21}\text{Ga}_{0.79}\text{As}/\text{GaAs}$ multiple quantum wells: A modified Pässler model for the S-shaped temperature dependence of photoluminescence energy », *Superlattices Microstruct.*, vol. 102, p. 351-358, févr. 2017, doi: 10.1016/j.spmi.2016.12.051.
- [33] Q. Li, S. J. Xu, M. H. Xie, et S. Y. Tong, « A model for steady-state luminescence of localized-state ensemble », *EPL Europhys. Lett.*, vol. 71, n° 6, p. 994, août 2005, doi: 10.1209/epl/i2005-10170-7.
- [34] Z. Su *et al.*, « A generalized model for time-resolved luminescence of localized carriers and applications: Dispersive thermodynamics of localized carriers », *Sci. Rep.*, vol. 7, no 13, p. 994, 02 February 2017, doi: 10.1038/s41598-017-00065-3.
- [35] Q. Li *et al.*, « Thermal redistribution of localized excitons and its effect on the luminescence band in InGaN ternary alloys », *Appl. Phys. Lett.*, vol. 79, n° 12, p. 1810-1812, sept. 2001, doi: 10.1063/1.1403655.
- [36] Z. C. Su *et al.*, « Electroluminescence probe of internal processes of carriers in GaInP single junction solar cell », *Sol. Energy Mater. Sol. Cells*, vol. 168, p. 201-206, août 2017, doi: 10.1016/j.solmat.2017.04.041.

- [37] H. Wang et al., « Direct correlation of defects and dark currents of InGaAs/ InP photodetectors», Mat. Sci. Semicon. Proc., Vol. 123, no 1, p. 105540, march 2021,doi: 10.1016/j.mssp.2020.105540.
- [38] M.YuI, et al., «Interdot carrier transfer in asymmetric bilayer InAs/GaAs quantum dot structures», Appl. Phys. Lett. vol.86, no 6, p. 063102, mars 2005, doi: 10.1063/1.1861980.
- [39] R. K. Ahrenkiel et al., «Recombination lifetime of In_{0.53}Ga_{0.47}As as a function of doping density», Appl. Phys. Lett. vol.72, no 26, p. 3470, April 1998, doi: 10.1063/1.121669.
- [40] B. Deveaud et al «Enhanced radiative recombination of free excitons in GaAs quantum wells», Phys. Rev. Lett., vol. 67, no 10, p. 2355, octobre 1991, doi: 10.1103/PhysRevLett.67.2355.
- [41] I. Fraj et al., «optical investigation of In_{0.21}Ga_{0.79}As multiple quantum wells grown on (001) and (113) A GaAs substrates», Superlattices Microstruct. vol.82, no 6, p. 406-414, june 2015, doi: 10.1016/j.spmi.2015.02.034
- [42] Y. Shi et al., «Time-Resolved Photoluminescence Characterization of InGaAs/GaAs Nano-Ridges Monolithically Grown on 300 mm Si Substrates», J. Appl. Phys., vol. 127, no 10, p. 1031404, march 2020, doi: 10.1063/1.5139636.